Applied Catalysis B: Environmental 100 (2010) 173–178

Contents lists available at ScienceDirect

Applied Catalysis B: Environmental

journal homepage: www.elsevier.com/locate/apcatb

Synthesis of $ZnWO_4$ nanorods with [1 0 0] orientation and enhanced photocatalytic properties

Rui Shi, Yajun Wang, Di Li, Jing Xu, Yongfa Zhu*

Department of Chemistry, Tsinghua University, Beijing 100084, China

ARTICLE INFO

Article history:
Received 5 May 2010
Received in revised form 19 July 2010
Accepted 24 July 2010
Available online 3 August 2010

Keywords:
Photocatalyst
$ZnWO_4$
Nanorods
Active planes

ABSTRACT

$ZnWO_4$ photocatalysts with various morphologies were synthesized by a template-free hydrothermal synthesis process. The morphologies had a significant influence on the photocatalytic activity for methylene blue and Rhodamine B degradation. $ZnWO_4$ nanorods with a highly [1 0 0] preferred orientation, obtained at pH 10, exhibited the highest photocatalytic activity among all the samples. This kind of nanorods had the most planes along the [1 0 0] direction—(0 1 0) and (0 1 1) planes, which meant most (0 1 0) and (0 1 1) planes exposed in $ZnWO_4$ phase. Basis on the analysis of crystal plane and hydrogen-related defects, the (0 1 0) and (0 1 1) planes could speculate to be more active for photodegradation.

1. Introduction

Semiconductor photocatalysts nanocrystals with tailored shaped have attracted intense research interest in the past decade due to their many intrinsic shape-dependent properties [1–7]. The surface structure of photocatalysts plays an important role to their photocatalytic activities because the photocatalytic reaction takes place only when photoinduced electrons and holes are available on the surface [8,9]. For example, theoretical and experimental studies indicated that the (0 0 1) surface of anatase TiO_2 is much more reactive than the thermodynamically more stable (1 0 1) surface and that the (0 0 1) surface may in fact be the dominant source of active sites for various applications [10–12]. Therefore, the surface controlled fabrication of nanocrystals is not only a rational route to study the relations between the surface structures and the photocatalytic properties but also a feasible approach for developing highly active photocatalysts.

$ZnWO_4$ as a kind of tungstate has received considerable attention due to its applications as an X-ray and γ-scintillator, photoanodes, and solid-state laser host, as well as for acoustic and optical fibers [13]. Our previous research showed that $ZnWO_4$ exhibited relatively high photocatalytic and photoelectrocatalytic activities for the mineralization of organic compounds [14–16]. However, further research on the relationship between reactive planes and photocatalytic activity has been not reported. There were several methods for the preparation of $ZnWO_4$, including solid-state reaction, the sol–gel method, the polymerized complex method and the hydrothermal method [13,17–19]. The hydrothermal method was an easy method to control the morphology and crystal growth orientation. Obviously, this suitable synthetic approach may give rise to differing photochemical properties due to possible variation of surface morphology and structure. Recently, our group demonstrated the synthesis of monoclinic-$ZnWO_4$ (*m*-$ZnWO_4$) nanostructures by a hydrothermal process, combined with the introduction of cetyltrimethyl ammonium bromide (C_{16}TAB) as surfactant. However, owing to the remained C_{16}TAB in the surface of $ZnWO_4$, the photocatalytic activities were not high [16]. Hence, using template- and surfactant-free solution routes for the preparation of uniform, high-purity *m*-$ZnWO_4$ nanocrystals with controllable crystallographic planes is indispensable.

In this work, $ZnWO_4$ photocatalysts with different morphologies were synthesized by the hydrothermal method without any template. Both the aqueous methylene blue (MB) and Rhodamine B (RhB) photodegradation were employed as the probe reaction to test the photocatalytic activity of the as-prepared samples under UV irradiation. We found that more (0 1 0) and (0 1 1) planes along [1 0 0] direction exposed in $ZnWO_4$ nanorods. And these $ZnWO_4$ nanorods exhibited greatly enhanced activity in the photocatalytic degradation of organic contaminants. As far as we know, this was the first attempt to reveal the relationship between reactive planes and photocatalytic activity of $ZnWO_4$.

* Corresponding author. Tel.: +86 10 62783586; fax: +86 10 62787601.
E-mail address: zhuyf@tsinghua.edu.cn (Y. Zhu).

0926-3373/$ – see front matter © 2010 Elsevier B.V. All rights reserved.
doi:10.1016/j.apcatb.2010.07.027

2. Experimental

2.1. Synthesis of sample

$ZnWO_4$ samples were prepared through a hydrothermal process. All chemicals used were analytic grade reagents without further purification. $Zn(NO_3)_2$ and Na_2WO_4 (1:1 molar ratio) were mixed together, and then 40 mL of distilled water was added. White precipitates appeared immediately, and the beaker was placed in an ultrasonic bath for 30 min to complete the precipitation reaction. The precipitates were filtered off, washed several times, and then added to stainless steel autoclaves with a Teflon liner containing a mixed solution of 30 mL of distilled water. Finally, the pH was adjusted to a specific value using $NH_3{\cdot}H_2O$ or HNO_3 solution. After being sealed, the autoclaves were heated in a convection oven at 180 °C. The products were collected by filtration and washed by distilled water several times. The samples were then dried at 60 °C for 8 h before characterization.

2.2. Characterization

Purity and crystallinity of the as-prepared sample was characterized by XRD on Bruker D8-advance diffractometer using Cu Kα radiation (λ = 1.5418 Å). The XRD data for indexing and cell-parameter calculation were collected in a scanning mode with a step length of 0.02° and a preset time of 5.6 s/step. Morphologies and structure of the as-prepared samples were further examined with transmission electron microscopy (TEM) by a JEM 1010 electron microscope operated at an accelerating voltage of 100 kV. High resolution transmission electron microscopy (HRTEM) images were obtained by JEM 2010F field emission gun transmission electron microscope operated at an accelerating voltage of 200 kV. The Brunauer–Emmett–Teller (BET) surface area was measured by ASAP 2010 V5.02H. Total organic carbon (TOC) was measured with a Tekmar Dohrmann Apollo 9000 TOC analyzer. Fourier transform infrared spectra (FT-IR) were recorded on a Perkin-Elmer 1600 FT-IR spectrometer with a KBr disk.

2.3. Photocatalytic test

The photocatalytic activities of sample were evaluated by degradation of MB and RhB under ultraviolet light irradiation of an 11 W low-pressure lamp with 254 nm. The average light intensity was 0.9 mW/cm^2. The radiant flux was measured with a power meter from the Institute of Electric Light Source (Beijing). MB and RhB solution (100 mL, 1.0×10^{-5} mol/L) containing 50 mg of as-prepared samples were placed in a glass beaker. Before the light was turned on, the solution was stirred for 30 min to ensure equilibrium between the catalysts. Volumes of 3 mL of sample solution were taken at given time intervals and separated through centrifugation. The supernatants were analyzed by recording variations of the absorption band maximum in the UV–vis spectra using a U-3010 spectrophotometer (Hitachi).

3. Results and discussion

3.1. Catalyst characterization

Fig. 1 showed XRD patterns for the samples prepared at different pH value for 24 h. Clearly, the pH value of the precursor medium had a crucial effect on the formation of $ZnWO_4$. At a low pH (pH <4) value, the formation of tungstic acid $WO_3(H_2O)_{0.33}$ phase was favorable (JCPDS Card number: 72-0199). This indicated that the optimal pH value for the formation of $ZnWO_4$ by this method was above pH ≥4. When the pH value was 4, the crystalline phase

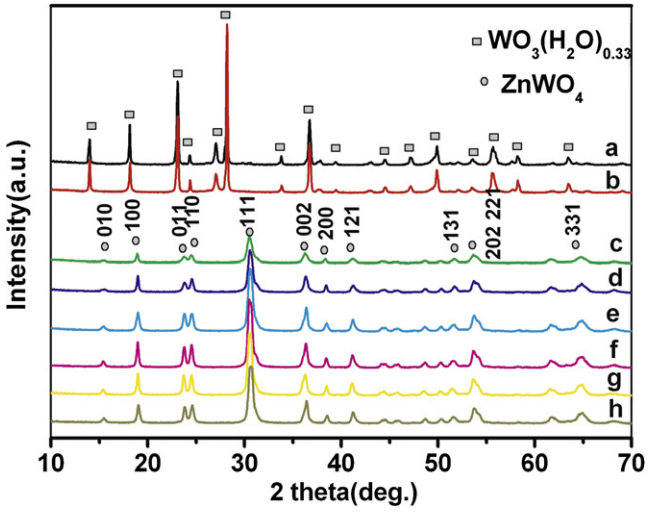

Fig. 1. XRD patterns for the samples prepared at different pH value for 24 h: (a) 1, (b) 2, (c) 4, (d) 6, (e) 8, (f) 10, (g) 12 and (h) 14.

of $ZnWO_4$ appeared, which could be easily indexed as a monoclinic wolframite tungstate structure according to the standard card (JCPDS Card number: 73-0554). The crystalline phase became perfect with the increase of pH value. According to the JCPDS Card number: 73-0554, the standard intensity of the (1 0 0) peak is about 3.7 times that of the (0 1 0) peak, which could be expressed as $I(1\,0\,0)/I(0\,1\,0) = 3.7$. In the XRD pattern of the sample prepared at pH 10 for 24 h, the value of $I(1\,0\,0)/I(0\,1\,0) = 6.3$. It implied the crystal had special anisotropic growth along the [1 0 0] direction, which was consistent with literature [20,21]. This conclusion was further confirmed by HRTEM observation below.

The morphologies and microstructures of the as-prepared $ZnWO_4$ were then investigated with TEM. Fig. 2 showed that the morphologies and dimensions of the $ZnWO_4$ were strongly dependent on pH value. Fig. 2(a) showed the TEM micrograph for the sample prepared at pH 4, from which we can see that some granular structure appeared. With the increase of the pH value to 6, the mixture of granular and rod-shaped crystals can be seen (Fig. 2(b)). For pH value of 8, the crystal grew to form a nanorod structure with an obviously preferred orientation (Fig. 2(c)). When the pH value was raised to 10, the rod-shaped crystals grew longer and a majority of the crystals had exceeded 200 nm in length (Fig. 2(d)). With the pH value further increasing, $ZnWO_4$ nanorods decreased in length, but increased in diameter (Fig. 2(e)). This phenomenon was especially notable when the sample was prepared at pH 14 (Fig. 2(f)). Obviously, the sample prepared at pH 10 showed the maximal aspect ratio.

To understand the preferential orientation growth, $ZnWO_4$ nanorod prepared at pH 10 had been further studied using HRTEM, and the results were shown in Fig. 3. The HRTEM images (Fig. 3(a) and (b)) showed that the nanorods are straight and perfect over their entire lengths. The lattice spacing of orthogonal lattice 0.37 and 0.47 nm corresponded to the (0 1 1) and (1 0 0) planes of the $ZnWO_4$, respectively (Fig. 3(a)). The lattice spacing of 0.58 nm appeared corresponded to (0 1 0) plane at another nanorod (Fig. 3(b)). The selected area electron diffraction (SAED) pattern (Fig. 3(c)) taken from a single nanorod revealed the single-crystalline nature of the nanorods. So the nanorods grew preferentially along the [1 0 0] direction, which was parallel to the (0 1 1) and (0 1 0) faces.

According to experiment result, the growth of $ZnWO_4$ nanorod under the hydrothermal conditions was possibly subjected to the Gibbs–Thomson mechanism, which was consistent with the result of reference [20,22]. The whole process of the nanorod growth in

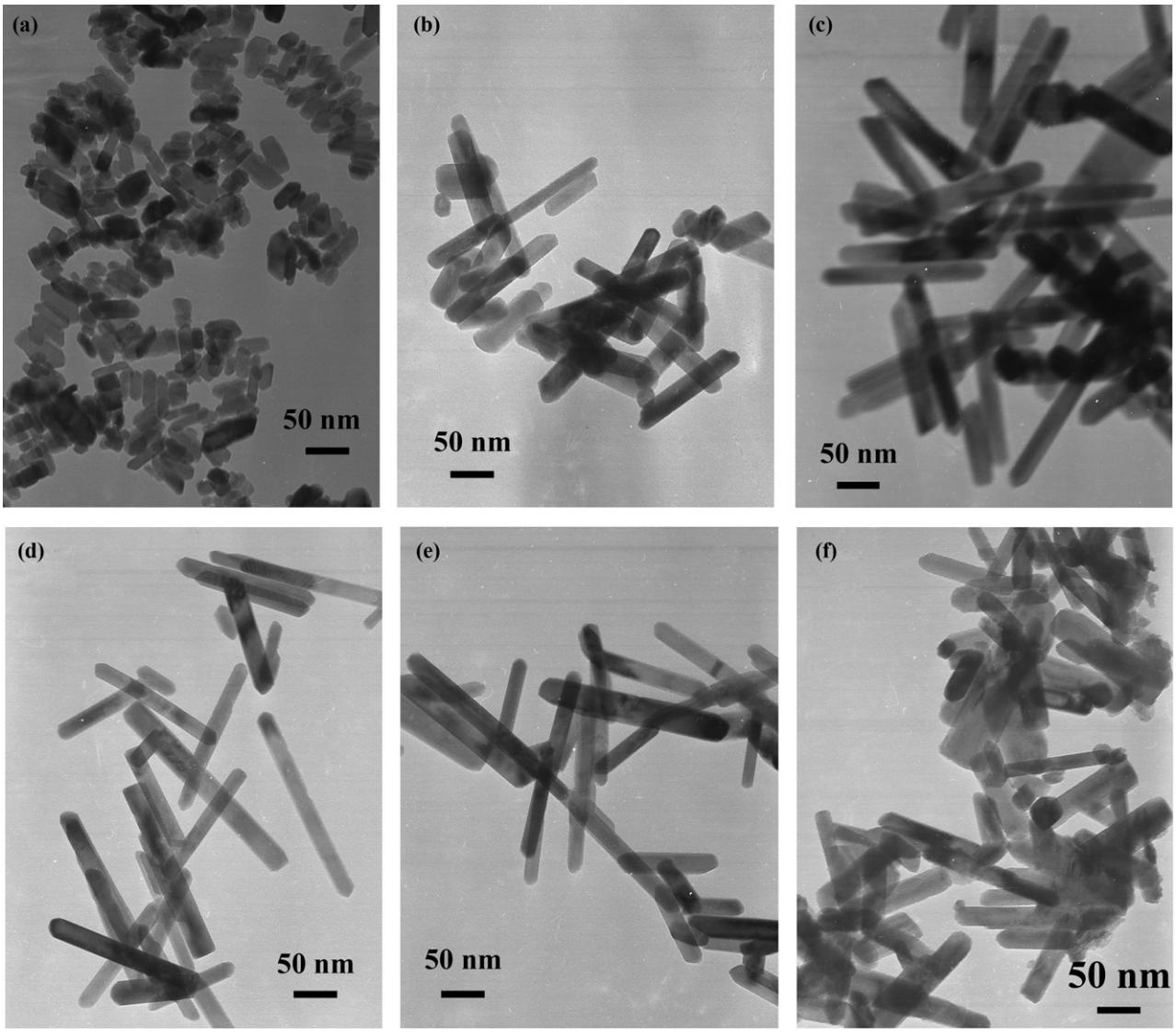

Fig. 2. TEM images for the samples prepared at different pH value for 24 h: (a) 4, (b) 6, (c) 8, (d) 10, (e) 12 and (f) 14.

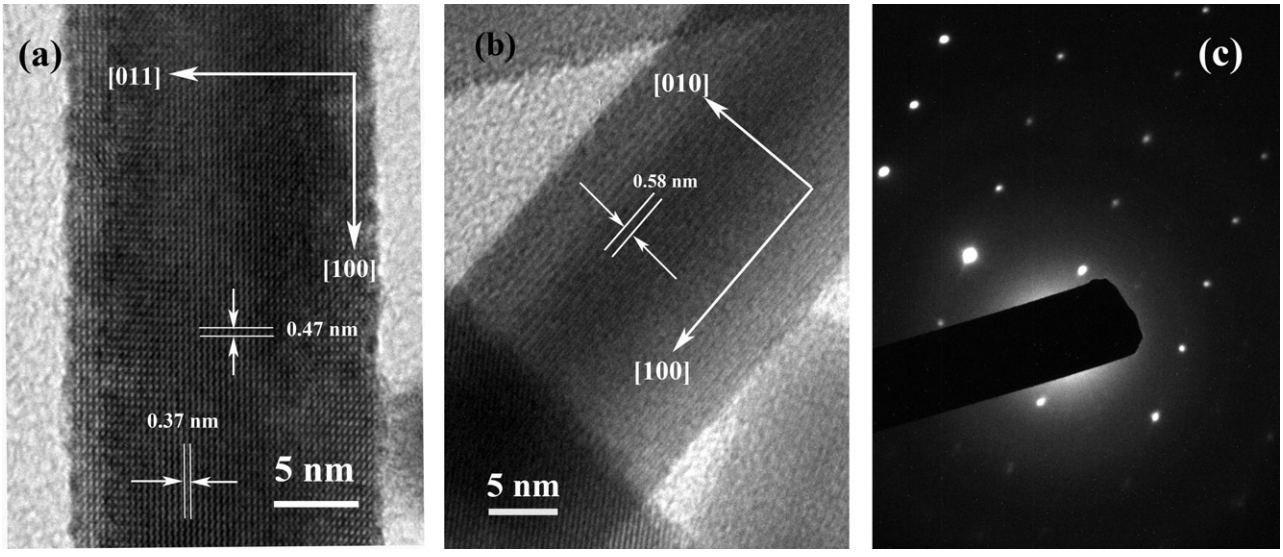

Fig. 3. (a and b) HRTEM images of the samples prepared at pH value of 10 for 24 h. (c) EDAX pattern of the single nanorod.

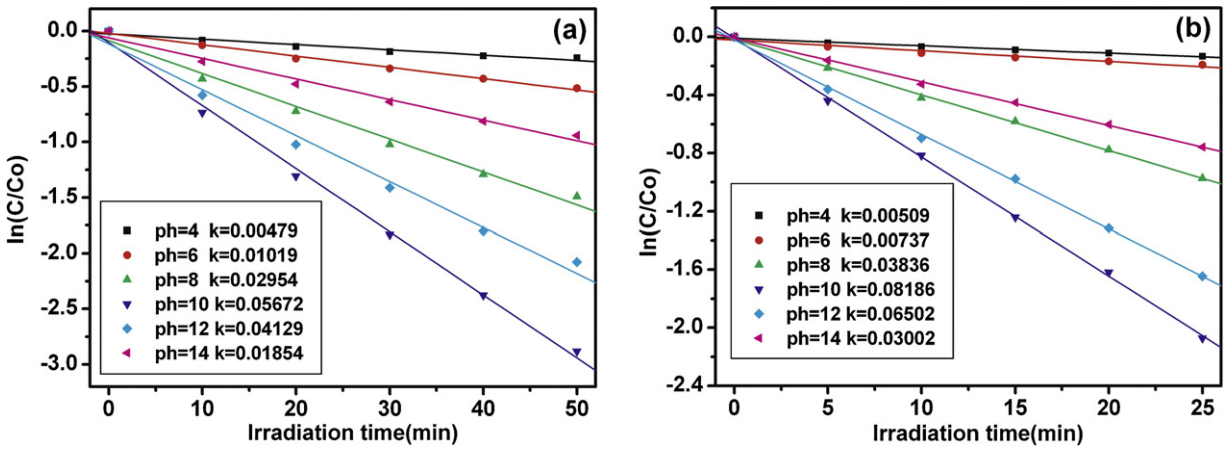

Fig. 4. Photocatalytic degradation of MB (a) and RhB (b) under UV irradiation by the samples prepared at different pH value for 24 h.

detail was obtained by TEM observation of the time series samples treated at pH value of 10 (see Supporting Information Fig. S1).

3.2. Photocatalytic activity

On the basis of the surface characterization results described above, it is now instructive to compare the photocatalytic activities of all $ZnWO_4$ samples under UV light irradiation. First, the MB photodegradation was tested as a model reaction to evaluate photocatalytic activities. The results were shown in Fig. 4(a). The MB photodegradation over the catalysts was fitted for pseudo-first-order kinetics. The pH value had a significant effect on the degradation rate. The determined reaction rate constant (k) was 0.00479, 0.01019, 0.02954, 0.05672, 0.04129 and 0.01854 min^{-1}, respectively, for the samples prepared at pH 4, 6, 8, 10, 12 and 14. In the range 4–10, an increase in the pH value resulted in the acceleration of MB degradation. The sample prepared at pH value of 10 showed the highest photoactivity. MB could be degraded less than 50 min. However, the sample prepared at pH value of 12 revealed the lower activity to degrade MB. When the pH value further increased, the activity decreased markedly.

To further evaluate the photocatalytic activity of $ZnWO_4$, we also studied the RhB degradation over the as-prepared samples. The results were shown in Fig. 4(b). It was obvious that RhB could be well degraded and reaction rate was faster than that of MB. Similar to MB degradation, the photocatalytic activity of samples for decomposition of RhB also depended on the pH value, and the best performance was also realized on pH value of 10, about 90% of the RhB was degraded in 25 min. Previously, our group had reported the synthesis of $ZnWO_4$ nanorod through C_{16}TAB surfactant, and found the $ZnWO_4$ nanorod could degrade the RhB under UV light irradiation. However, owing to the remained C_{16}TAB on the surface of photocatalysts, the photocatalytic activities were not high [16]. In our work, the morphlolgies of $ZnWO_4$ nannstructure could be well controlled though template-free synthesis. Moreover, the photocatalytic activity increased about 2–3 times for degradation of RhB.

In order to further understand the mineralization property of the photocatalyst, the decrease of TOC in the photodegradation of MB and RhB by $ZnWO_4$ nanorod prepared in pH 10 was illustrated in Fig. 5. Obviously, the rate of TOC reduction was slower than that of the degradation of the dye, suggesting that the cleavage breakage of conjugated chromophore ring of MB and RhB resulted in the intermediates occurring during the photocatalytic process. When 90% of dyes were transformed, about 44 and 50% of mineralized degree were reached, respectively, for MB and RhB. And also, the photocatalytic degradation and mineralization of MB and RhB was significantly improved by the presence of O_2 bubbling, indicating O_2 was a key factor in the photocatalytic process (see Supporting Information Fig. S2).

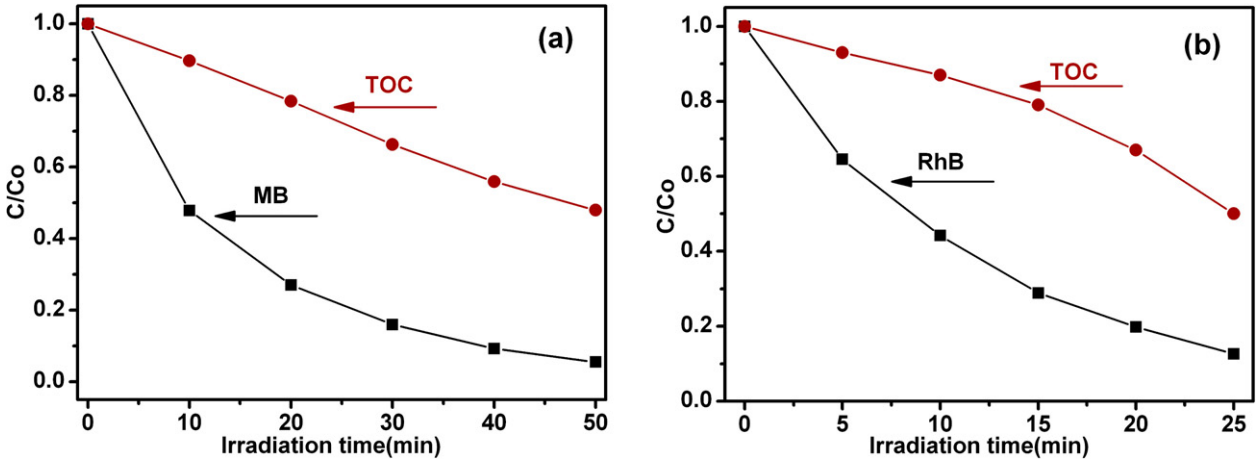

Fig. 5. Changes in MB (a) and RhB (b) concentration and TOC under UV irradiation by the samples prepared at pH value of 10 for 24 h.

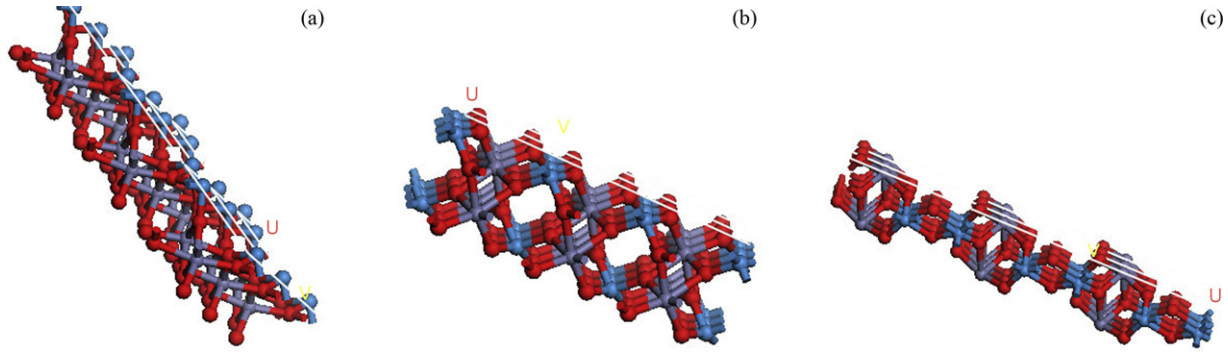

Fig. 6. Structure of $ZnWO_4$ (a) (1 0 0)-3 × 3, (b) (0 1 0)-3 × 3 and (c) (0 1 1)-3 × 3 surface. The O atoms are in red, W in blue and Zn in violet. (For interpretation of the references to color in this figure legend, the reader is referred to the web version of the article.)

3.3. *Effect of nanostructure on the photocatalytic activity*

Photocatalytic activities for decomposing MB and RhB were found to be dependent on morphologies of samples. The activity increased with increasing nanorods' aspect ratio. $ZnWO_4$ nanorods with maximal aspect ratio, obtained at pH 10, exhibited the highest photocatalytic activity among all the samples.

According to HRTEM results (Fig. 3), most (0 1 0) and (0 1 1) planes along the [1 0 0] direction exposed in $ZnWO_4$ nanorods prepared at pH 10, and nanoparticles had no obvious crystal orientation. In the attempt to explore the effect of planes on the photocatalytic activity, we examined the $ZnWO_4$ (1 0 0) surface, which was the end surface of the nanorods (Fig. 6(a)). For comparison, the $ZnWO_4$ (0 1 0) and (0 1 1) surface were also shown in Fig. 6(b) and (c). As one can see, $ZnWO_4$ (1 0 0) exposed almost all coordinatively unsaturated W atom. Previous studies by Kanan SM and coworkers had shown monoclinic tungsten oxide (m-WO_3) surfaces contained a large amount of hydroxyl groups at room temperature [23]. So we can believed that surface hydroxyl groups would easily form on $ZnWO_4$ (1 0 0) surface. However, $ZnWO_4$ (0 1 0) exposed coordinatively unsaturated W and O atom (Fig. 6(b)). It was noteworthy that a smaller proportion of unsaturated W atom was observed in (0 1 0) than that in (1 0 0) surfaces. As a consequence, the chance of surface hydroxyl groups formation in (0 1 0) would be less than that in (1 0 0) surfaces. Similar to (0 1 0) surfaces, (0 1 1) surfaces contained both unsaturated Zn atom and O atom as shown in Fig. 6(c). So the maximum probability of surface hydroxyl group formation could be also realized on (1 0 0) surface. According to the TEM results discussion above, $ZnWO_4$ nanorods grew longer with the increase of the pH value from 4 to 10, which meant nanorods had more (0 1 0) and (0 1 1) planes along the [1 0 0] direction. Consequently, $ZnWO_4$ nanorods prepared at pH value of 10, theoretically, would have a lowest density of surface hydroxyl groups.

Table 1
BET surface area of $ZnWO_4$ samples prepared at different pH value for 24 h.

Sample	pH 4	pH 6	pH 8	pH 10	pH 12	pH 14
BET surface area (m^2/g)	36.3	30.0	25.6	23.4	18.3	9.2

FT-IR analyses of the series samples were performed to practically examine the surface hydroxyl groups in $ZnWO_4$ nanocrystal (as shown in Fig. 7). There were two peaks at 3447 and 1620 cm^{-1} in the FT-IR spectra of all samples, implying that the basic hydroxyl groups existed in all $ZnWO_4$ samples and the surface of samples was hydroxylated. Furthermore, the intensity of absorption peak of surface hydroxyl groups decreased with increasing pH value from 4 to 10, which was in good agreement with the analysis on crystal planes above. However, the intensity of hydroxyl groups for sample prepared at pH value of 14 dropped obviously, which seemed to be contradictory with the analysis on crystal planes. Note that synthesis of $ZnWO_4$ at pH value above 12 largely caused loss of surface area of the sample (Table 1); as a result, the sample prepared at pH value of 12 or 14 had lower population of surface hydroxyl groups.

During the hydrothermal synthesis process, a certain mount of surface hydroxyl groups existed in the sample, as we have known, which will lead to the formation of hydrogen-related defects

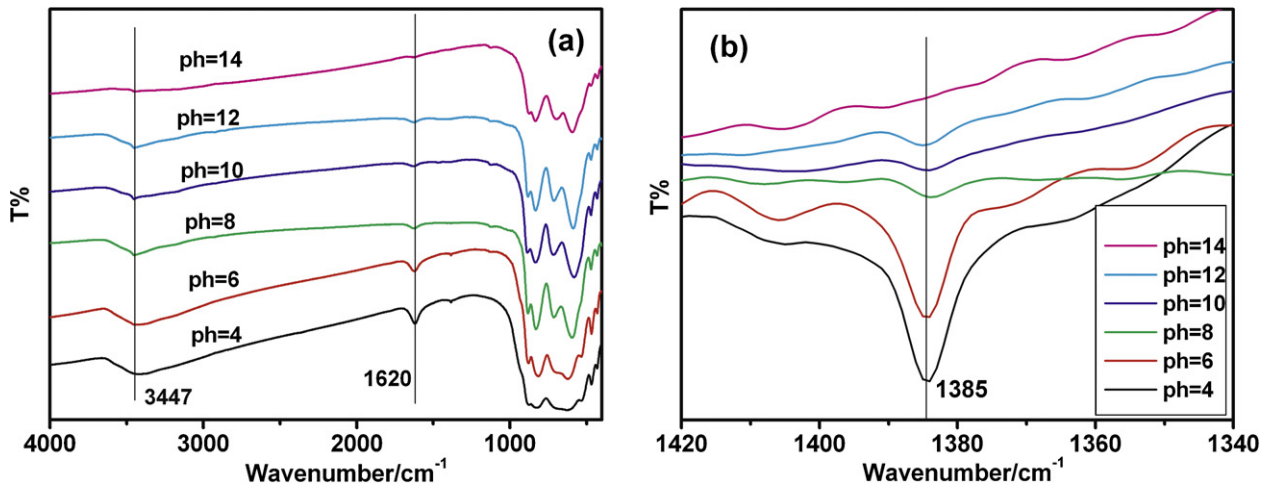

Fig. 7. (a) FT-IR spectra of $ZnWO_4$ prepared at different pH value for 24 h. (b) A careful comparison in the range of 1420–1340 cm^{-1}.

[24,25]. In general, defects may act as recombination centers for photoinduced electrons and holes, reducing the total photocatalytic activity significantly. Hence, defects in the crystal structure are considered as an important factor influencing the photocatalytic activity. A careful comparison in the IR peak at 1385 cm^{-1}, where hydrogen-related defects modes were expected [25], were shown in Fig. 7(b). The intensities of hydrogen-related defects decreased with the increase of pH value from 4 to 10, indicating the number of hydrogen-related defects was decreasing. Moreover, as we have known, in the range 4–10, an increase in the pH value resulted in the acceleration of degradation activity (as shown in Fig. 4). Hence, it was to be believed that $ZnWO_4$ nanorods prepared at pH value of 10 possessing the highest photocatalytic activity could be ascribed to the lowest hydrogen-related defects. The lowest intensity at 1385 cm^{-1} for sample prepared at pH value of 14 was due to the smallest surface area as discussing above. Furthermore, the smallest surface area could restrict its photocatalytic activity more or less.

In conclusion, during the hydrothermal synthesis process, different morphologies of $ZnWO_4$ photocatalyst would be formed, thereby, possessing different crystal orientation. $ZnWO_4$ nanorods with maximal aspect ratio, had most (0 1 0) and (0 1 1) planes along the [1 0 0] direction. Moreover, hydrogen-related defects could be hardly formed in these planes; as a result, this sample exhibited the highest photocatalytic activity among all the samples. Therefore, the (0 1 0) and (0 1 1) planes along the [1 0 0] direction could speculate to be more active for photodegradation.

4. Conclusion

The morphologies of $ZnWO_4$ could be easily controlled through a template-free hydrothermal synthesis process. $ZnWO_4$ nanorods with a highly [1 0 0] preferred orientation were obtained at pH value of 10. The photocatalytic activity of nanorod was higher than that of the other samples. The [1 0 0] preferred orientation growth of the nanorods could reduce the hydrogen-related defects and enhance the photocatalytic activity of $ZnWO_4$ catalyst.

Acknowledgments

This work was partly supported by the National Natural Science Foundation of China (20925725 and 50972070) and National Basic Research Program of China (2007CB613303).

Appendix A. Supplementary data

Supplementary data associated with this article can be found, in the online version, at doi:10.1016/j.apcatb.2010.07.027.

References

[1] N. Tian, Z. Zhou, S. Sun, Y. Ding, Z. Wang, Science 316 (2007) 732.
[2] Y. Yin, A. Alivisators, Nature 437 (2005) 664.
[3] C. Wang, H. Daimon, T. Onodera, T. Koda, S. Sun, Angew. Chem. Int. Ed. 47 (2008) 3588.
[4] A. Tao, S. Habas, P. Yang, Small 4 (2008) 310.
[5] Y. Jun, J. Choi, J. Cheon, Angew. Chem. Int. Ed. 45 (2006) 3414.
[6] C. Zhang, Y. Zhu, Chem. Mater. 17 (2005) 3537.
[7] H. Fu, C. Pan, W. Yao, Y. Zhu, J. Phys. Chem. B 109 (2005) 22432.
[8] A. Hameed, T. Montini, V. Gombac, P. Fornasiero, J. Am. Chem. Soc. 130 (2008) 9658.
[9] J. Zhang, Q. Xu, Z. Feng, M. Li, C. Li, Angew. Chem. Int. Ed. 47 (2008) 1766.
[10] H. Yang, C. Sun, S. Qiao, J. Zou, G. Liu, S. Smith, H. Cheng, G. Lu, Nature 453 (2008) 638.
[11] H. Yang, G. Liu, S. Qiao, C. Sun, Y. Jin, S. Smith, J. Zou, H. Cheng, G. Lu, J. Am. Chem. Soc. 131 (2009) 4078.
[12] X. Han, Q. Kuang, M. Jin, Z. Xie, L. Zheng, J. Am. Chem. Soc. 131 (2009) 3152.
[13] M. Bonanni, L. Spanhel, M. Lerch, E. Fuglein, G. Muller, Chem. Mater. 10 (1998) 304.
[14] H. Fu, J. Lin, L. Zhang, Y. Zhu, Appl. Catal. A 306 (2006) 58.
[15] X. Zhao, Y. Zhu, Environ. Sci. Technol. 40 (2006) 3367.
[16] J. Lin, J. Lin, Y. Zhu, Inorg. Chem. 46 (2007) 8372.
[17] A. Phani, M. Passacantdando, L. Lozzi, S. Santucci, J. Mater. Sci. 35 (2000) 4879.
[18] J. Ryu, C. Lim, K. Auh, Mater. Lett. 57 (2003) 1550.
[19] F. Wen, X. Zhao, H. Huo, J. Chen, E. Lin, J. Zhang, Mater. Lett. 55 (2002) 152.
[20] S. Yu, B. Liu, M. Mo, J. Huang, X. Liu, Y. Qian, Adv. Funct. Mater. 13 (2003) 639.
[21] B. Liu, S. Yu, L. Li, F. Zhang, Q. Zhang, M. Yoshimurra, P. Shen, J. Phys. Chem. B 108 (2004) 2788.
[22] J. Mullin, Crystallization, 3rd ed., Butterworth-Heinemann, Oxford, UK, 1997.
[23] S. Kanan, Z. Lu, J. Cox, G. Bernhardt, C. Tripp, Langmuir 18 (2002) 1707.
[24] H. Chen, Y. Chen, Ind. Eng. Chem. Res. 42 (2003) 473.
[25] Z. Li, T. Yu, Z. Zou, J. Ye, Appl. Phys. Lett. 88 (2006) 071917.